

Robotic Intracellular Pressure Measurement Based on Improved Balance Pressure Model

Jinyu Qiu, Minghui Li, Ruimin Li, Yue Du, *Member, IEEE*, Yaowei Liu, *Member, IEEE*, Mingzhu Sun, *Member, IEEE*, Xin Zhao, *Member, IEEE*, Qili Zhao*, *Member, IEEE*,

Abstract—Intracellular pressure regulates cell physiological activities and impacts cell micromanipulation results. The measurement of intracellular pressure may reveal the mechanism of these cell physiological activities and improve the micromanipulation accuracy for cells. Current intracellular pressure measurement methods usually rely on specialized and expensive devices or have significant cytotoxicities on cells. In this paper, a simple robotic intracellular measurement method based on an improved balance pressure model is developed on the traditional cell manipulation system setup. First, an improved balance pressure model is proposed to calculate the intracellular pressure. Then, a traditional glass micropipette is utilized as a probe to penetrate the cell membrane to measure intracellular pressure. After cell membrane penetration, the key parameters of the improved balance pressure model including the cell deformation and the moving distance of the gas-liquid interface (GLI) inside the micropipette are measured in time to calculate the intracellular pressure. The experimental results on porcine oocytes demonstrate that the proposed method has an 80% success rate at an average measurement speed of 12 seconds/cell. Further, no intracellular pressure leaking was tested during the measurement process, guaranteeing measurement accuracy. Further, an 87.5% survival rate of operated oocytes was obtained after the measurement, proving limited damage to cell viability. Our method is highly expected to be applied in biological applications requiring in situ measurement of intracellular pressure.

Index Terms—Intracellular pressure measurement, robotic cell manipulation, micromanipulation.

I. INTRODUCTION

CELLS can maintain positive intracellular pressure compared to the extracellular environment. Intracellular pressure is an important component of the intracellular environment, which ensures the normal physiological function of cells. It is also the main source of mechanical stimulation to intracellular structures such as organelles [1] and plays an important role in cell division [2], [3], differentiation [4], [5], migration [6], diseases [7], [8] and embryonic tissue development [9], [10]. Besides, intracellular pressure affects the results of cell micromanipulation. For example, the positive intracellular pressure hinders the delivery of injected materials,

resulting in a lower deposition volume of cell microinjection [11], [12]. In addition, the existence of intracellular pressure generates a force that supports cells' swell, making cell surface "feel" harder from the outside, which affects the measurement results of cell mechanical properties such as cell elasticity. Therefore, intracellular pressure measurement is beneficial for revealing the mechanism of cell physiological activities and improving the accuracy of cell micromanipulation.

Some methods have been reported to measure the intracellular pressure of cells. Intracellular pressure was first estimated indirectly from the cortical tension of cells, according to Laplace's law [13], [14]. However, this method assumed the cell to be a liquid ball which makes it only effective for cells with thin membranes. For oocytes or embryos with thick zona pellucida (ZP), the measurement errors of this method may be too large to be applicable. The intracellular pressure has also been measured through the variations in the poking force-cell deformation curves obtained before and after the release of intracellular pressure [15]. Although this method is applicable for oocytes or embryos with thick ZPs, it used laser cutting to release intracellular pressure and microforce sensors to obtain the poking force-cell deformation curves. Thus, that method has a complex operation process and requires expensive equipment, significantly limiting its application. In previous research, we proposed a measurement method of intracellular pressure based on the modeled relationship between the applied pressure and the deposition volume of the oil injected into cells [12]. Although this method applies to traditional cell manipulation system setup, the oil droplets injected into the cells in this method have significant cytotoxicity to the viability of the cells. A commercial micro-pressure system from WPI with fast feedback control of the output pressure has been used to measure intracellular pressure [16]–[19]. The system used a micropipette electrode to penetrate the cell membrane, measured the electrode resistance variation and then compensated for it with fast adjustment of the output pressure. Then the variation of the output pressure is obtained to measure the intracellular pressure. Although this system can measure the intracellular pressure of a variety of cells and has limited harm to cell viability, its complicated operation process and the involved expensive devices for precise measurement of electrode resistance, such as the specified amplifier, significantly limit its widespread use. In summary, a simple intracellular pressure measurement method using traditional cell manipulation tools and with less harm to cell viability is still highly desired.

We previously proposed a balance pressure model at the gas

This research was jointly supported by the National Natural Science Foundation of China (62027812, 62273186) and the Beijing Advanced Innovation Center for Intelligent Robots and Systems under Grant 2019IRS05.

J. Qiu, M. Li, R. Li, Y. Du, Y. Liu, M. Sun, X. Zhao and Q. Zhao are with the Institute of Robotics and Automatic Information System (IRASIS), the Tianjin Key Laboratory of Intelligent Robotic (tjKLIR), Nankai University, Tianjin 300350, China, and Institute of Intelligence Technology and Robotic Systems, Shenzhen Research Institute of Nankai University, Shenzhen 518083, China. Q. Zhao is also with Beijing Advanced Innovation Center for Intelligent Robots and Systems, Beijing Institute of Technology, China.

*Contacting Author: Qili Zhao. (e-mail: zhaqili@nankai.edu.cn)

liquid interface (GLI) inside micropipette in which a positive injection pressure is applied to balance the extra negative pressure caused by the capillary effect (capillary pressure) and the hydrostatic pressure [20]. Using that model, the hydrostatic pressure can be calculated indirectly through capillary pressure and injection pressure. After the micropipette penetrates the cell membrane and enters the intracellular space, the hydrostatic pressure will be replaced by the intracellular pressure. In that case, the intracellular pressure may be calculated by the positive injection pressure and capillary pressure. However, the cell deformation and motion of the gas-liquid interface (GLI) resulting from the cell membrane penetration also affect the balance state of the above three pressures. Thus, an improved balance pressure model considering the above factors is required to measure intracellular pressure.

In this paper, a simple robotic intracellular pressure measurement method is developed based on an improved balance pressure model. First, an improved balance pressure model is established to calculate the intracellular pressure. Then, a traditional measurement micropipette with a sharpened tilt opening penetrates the cell membrane to measure the intracellular pressure. The key parameters of the improved balance pressure model including the cell deformation and moving distance of GLI were calculated in time by developed imaging processing methods to measure the intracellular pressure. Finally, a robotic measurement process of intracellular pressure is established based on the above work. The experimental results on porcine oocytes demonstrate that our method is capable of measuring intracellular pressure at an average speed of 12 seconds/cell with an 80% success rate. The measurement efficiency of our method is significantly higher than that of methods based on micropipette electrode resistance, which is expected to measure only dozens of cells at most per day [21]. Further, no intracellular pressure leaking was observed during the measurement process according to the diffusion results of the fluorescence injected into the cell, guaranteeing the measurement accuracy of the intracellular pressure. Further, an 87.5% survival rate of operated oocytes was obtained after measurement, proving limited damage to cells. More details of the comparison between our method with the other three methods are listed in Table I. Without the involvement of specific devices and having low damage to cell viabilities, our method is highly expected to achieve in situ measurement of intracellular pressure in biological applications.

II. SYSTEM SETUP

The robotic intracellular pressure measurement was performed using the in-house developed NKTY-MR601 micro-operation system [22]–[24]. As shown in Fig. 1, this system was built around an inverted microscope (CK-40, Olympus). A CCD camera (W-V-460, Panasonic) acquires microscope images at a speed of 30 frame/s. An in-house developed motorized X - Y stage (with a travel range of 100mm, a maximum speed of 2mm/s, and repeatability of $\pm 0.1\mu\text{m}$) was mounted on the microscope to position the oocytes. A pair of X - Y - Z micromanipulators (with a working space of 50mm \times 50mm \times 50mm, a maximum speed of 1mm/s, and

TABLE I
COMPARISON OF METHODS FOR MEASURING INTRACELLULAR PRESSURE

methods	reference [15]	reference [12]	micro-pressure system from WPI [19] [21]	this paper
technology	laser ablation	oil injection	sustaining concentration gradient at electrode tip	improved balance pressure model
equipment	micro-manipulators, biopsy laser and magnetic tweezer	micro-manipulators	micro-manipulators and micro-pressure system from WPI	micro-manipulators
cost	USD 500,000	USD 10,000	USD 100,000	USD 10,000
efficiency	/	20 cells/day	10 cells/day	20-30 cells/day
practice time	/	/	2 weeks	1 week
viability	/	0%	90%	87.5%

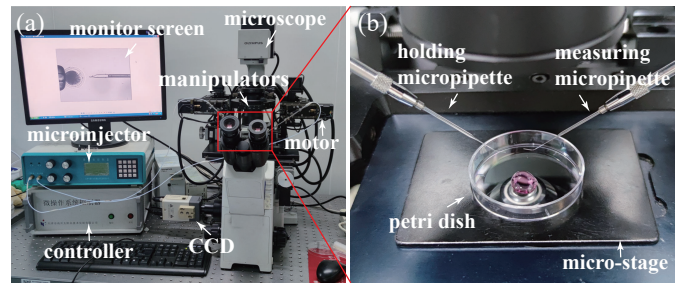


Fig. 1. Robotic intracellular pressure measurement system. (a) System setup. (b) Micro-operation workspace.

repeatability of $\pm 0.1\mu\text{m}$) were used to position the holding micropipette and the measurement micropipette. An in-house developed pneumatic pump provided the holding pressure (with a resolution of 10Pa) and injection pressure in the measurement. A host computer was utilized for microscopic image processing, pressure adjustment, motion control for the stage and manipulators. The holding micropipette was made from borosilicate glass tubes with an outer diameter of 1 mm and an inner diameter of 0.6mm. The holding micropipettes were pulled by the puller (MODEL P-97, Sutter Instrument) and fractured by the microforge (MF-900, NARISHIGE) to generate a micropipette with an inner diameter of 50–60 μm . Then, the holding micropipette was melted by the microforge to smooth the tip opening. The measuring micropipette was bought from Cooper Surgical (TPC, LBC-OD20BA90) with a slope angle of 45°.

III. KEY METHODOLOGIES AND TECHNOLOGIES

A. Improved Balance Pressure Model

When the micropipette is immersed in the culture medium, part of the culture medium will enter the micropipette to form a gas-liquid interface (GLI) under the effect of hydrostatic pressure, capillary force and injection pressure.

According to the interface mechanics [25], the capillary force F_c can be estimated by

$$F_c = \sigma 2\pi R \cos \beta \quad (1)$$

where R is the inner micropipette radius at the position of GLI, β is the contact angle between the GLI and the inner micropipette surface, and σ is the coefficient of surface tension of the liquid, which was measured by the abruption method [20].

The compressing force F_m of the inner surface to the liquid can be estimated by

$$F_m = \pi(R^2 - R_0^2)P_{in} \quad (2)$$

where P_{in} is the intracellular pressure and R_0 is the inner radius of the micropipette at the opening.

The intracellular pressure force F_{in} on the liquid inside the micropipette can be estimated by

$$F_{in} = \pi R_0^2 P_{in} \quad (3)$$

where P_{in} is the intracellular pressure. The injection force F_{inj} produced by the micropipette air pressure on the liquid can be estimated by

$$F_{inj} = \pi R^2 P_{inj} \quad (4)$$

In the balance state (see Fig. 2(a)), the above four forces satisfy the following equation:

$$F_{inj} = F_{in} + F_m + F_c \quad (5)$$

Substituting (1), (2), (3) and (4) into (5), the intracellular pressure is obtained as

$$P_{in} = P_{inj} - (2\sigma \cos \beta)/R \quad (6)$$

At the beginning of cell penetration, when the micropipette tip presses against the cell, the cell is deformed and the volume of the cell decreases (see Fig. 2(b)), which causes the increase in the intracellular pressure. After the micropipette tip penetrates the ZP, the intracellular pressure is released into the micropipette, which pushes the GLI far from micropipette tip (see Fig. 2(c)). With the recovery of cell deformation, the intracellular pressure decreases and the GLI moves back by a distance (see Fig. 2(d)).

The relationship between intracellular pressure, cell volume, and GLI moving distance before and after GLI movement can be written as

$$P_{in} V_{cell} = P_{in}' (V_{cell}' + \Delta L \pi R^2) \quad (7)$$

where P_{in} and V_{cell} are the actual intracellular pressure and volume of the cell before penetration, respectively. V_{cell}' is the volume of the cell after penetration and P_{in}' is the measured pressure inside the cell after penetration. ΔL is the moving distance of the GLI.

Besides, after the pipette tip penetrates the cell, the pipette and the liquid in it occupy part of the space inside the cell, which was misregarded as a change in the internal volume of the cell, and thus, needs to be excluded to calculate the actual volume of the cell. The relationship between intracellular

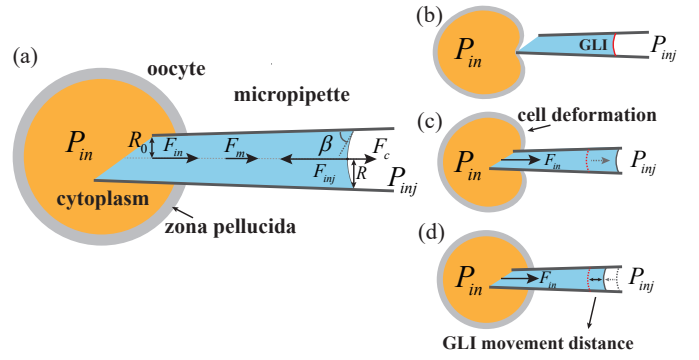


Fig. 2. The schematic of the intracellular pressure measurement process based on the improved balance pressure model. (a) The force analysis of the liquid in the micropipette. (b)-(d) Micropipette penetration process.

pressure, cell volume, GLI moving distance and pipette tip volume can be adjusted to be

$$P_{in} V_{cell} = P_{in}' (V_{cell}' + \Delta L \pi R^2 - V_{tip}) \quad (8)$$

where V_{tip} is the volume of intracellular space occupied by the pipette tip that penetrates the cell. For a pipette with a slope tip of 45° , the pipette volume pierced into the cell can be calculated as

$$V_{tip} = \pi R_0^3 + \pi R_0^2 L_{in} = \pi R_0^2 (R_0 + L_{in}) \quad (9)$$

where L_{in} is the length of the measurement pipette entering the intracellular space.

To eliminate the measurement error caused by cell deformation, the GLI position is detected when the detected cell deformation recovers ($V_{cell} = V_{cell}'$). In that case, the volume of the cell equals to that before penetration, and the relationship between the measured intracellular pressure after ZP penetration P_{in}' and the original intracellular pressure before ZP penetration P_{in} can be estimated by

$$P_{in} = \frac{V_{cell} + \pi R^2 \Delta L - V_{tip} P_{in}'}{V_{cell}} P_{in}' \quad (10)$$

Based on the improved balance model, substituting P_{in} in (6) into (10) as the measured pressure P_{in}' after penetration, the original intracellular pressure P_{in} can be obtained as

$$P_{in} = \frac{V_{cell} + \pi R^2 \Delta L - V_{tip}}{V_{cell}} (P_{inj} - (2\sigma \cos \beta)/R) \quad (11)$$

which indicates that the measurement of intracellular pressure requires the identification of the following key parameters: the cell deformation, the GLI moving distance, the micropipette inner radius, the radius of the cell, and the contact angle between GLI and the inner surface of the micropipette.

B. Determination of Measurement Micropipette Diameter

The diameter of the measurement micropipette was determined based on a comprehensive consideration of the identification of improved balance pressure model parameters and the prevention of intracellular pressure leakage during ZP penetration.

On the one hand, micropipettes with too small diameters were inappropriate for the intracellular pressure measurement

because of the following reasons. As aforementioned, the probing of intracellular pressure was based on the response of the GLI under the push of intracellular pressure, including GLI movement and contact angle changes. Limited by the imaging resolution of the acquired microscopic images, the relative error of measured contact angle β and micropipette radius R based on imaging processing for micropipettes with too small radius are larger, which further results in a larger measurement error of P_{in} according to (6).

On the other hand, too large micropipette dimensions may lead to intracellular pressure leakage from the large opening, necessitating the restriction of micropipette diameters to ensure that the ZP effectively seals the micropipette opening during penetration. To validate the sealing, the geometry of the ZP and the micropipette opening at the moment of penetration was analyzed. The shape of the ZP was fitted using the point-load model (equation (4) in reference [26]), taking into consideration that the micropipette makes contact with the ZP through its pointed tip. The relationship between the depth of the concave segment P_1P_2 of the ZP and its radius can be approximated by a parabolic model (12) with P_2 as the vertex (see Fig. 3(a)).

$$w = -\frac{w_d}{a^2}(a-r)^2 + w_d \quad (12)$$

where P_1 is the point of the micropipette tip, P_2 is the inflection point of the ZP, w_d and a correspond to the horizontal and vertical distances between P_1 and P_2 , respectively. P_1P_e is the sloped opening of the micropipette. All of these aforementioned parameters were obtained through image processing of the cell and micropipette. With the $20\mu\text{m}$ size micropipette in Fig 3(a), it is calculated that the entire parabolic curve at the depth of P_1P_2 lies above the line P_1P_e . This verifies that the contour of the ZP completely covers the micropipette opening at the moment of penetration. In the case of penetration experiments using a $30\mu\text{m}$ micropipette, the calculations indicated that the parabolic curve in this segment did not entirely lie above the micropipette's opening, leading to intracellular pressure leakage from the micropipette's tip to extracellular space (see Fig. 3(b)).

Based on the above considerations and calculations, the appropriate diameter of the measuring micropipettes for porcine oocytes was selected to be $20\mu\text{m}$.

C. Key Parameters Calculation for Improved Balance Model Based on Image Processing

As aforementioned in Section III(A), several key parameters of the improved balance pressure model need to be calculated to measure the intracellular pressure using the improved model. These parameters include the cell deformation, the GLI moving distance, the micropipette inner radius, the radius of the cell, and the contact angle between GLI and the inner surface of the micropipette. Among them, the calculation processes of the inner radius of the micropipette, cell radius, and contact angle have been introduced in detail in our previous published papers [20]. The readers may find more details about them in these references. In this section, we only focus on cell formation detection and GLI tracking as follows.

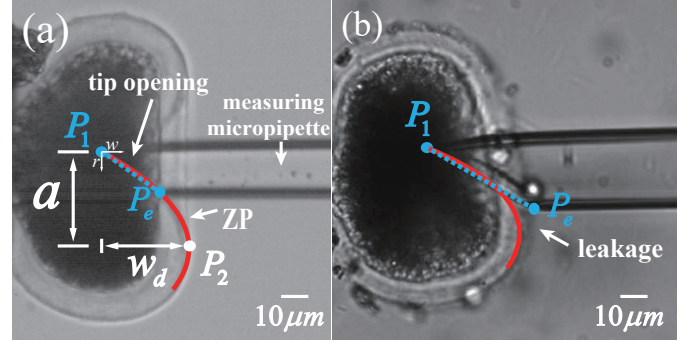


Fig. 3. Measurement micropipette diameter selection experiments. (a) A 20-micron diameter micropipette was used to penetrate the oocyte. (b) A 30-micron diameter micropipette was used to penetrate the oocyte.

1) *Cell deformation detection based on optical flow method*: Since the micropipette moves inside the focal plane of the cell and penetrates the cell along the central axis of the cell, the restoration of the intracellular area in the image was utilized to evaluate the restoration of cell deformation and intracellular space volume. The irregular edges of the cytoplasm generated after being contacted by the micropipette may cause significant measurement errors in the cytoplasm area. Addressing this problem, the cytoplasm area during penetration is estimated by the area enclosed by ZP, which is usually clearer, with the edge easily detected and less affected by cell deformation compared with the cytoplasm.

Before cell deformation, the outer contour and inner contour of ZP were detected by the Canny edge detector and Hough circle detector as introduced in our previous research [20], [27], [28], respectively. In this way, the ZP area was obtained and the pixels in ZP were determined for the following detection of the ZP area during ZP penetration. Then the micropipette squeezes the ZP, penetrates ZP, and retreats unless cell deformation fully recovers. During the above processes, the optical flows [29] of the pixels on the ZP were calculated from adjacent frames of cell images to track these pixels, and subsequently, determine the ZP area online. The cytoplasm area can be calculated through the area enclosed by the ZP area. The obtained ZP area in the above processes is shown in Fig. 4(a)-(d). The variation trend of cytoplasm area value is shown in Fig. 4(e). The squeezing stage, penetration moment, recovering stage, and total recovery moment can be founded in Fig. 4(e), which are in accordance with the operation process in Fig. 4(a)-(d). The above results demonstrate the feasibility of using cytoplasm area to estimate cell deformation.

2) *GLI moving distance calculation based on template matching*: The moving distance of the GLI is calculated through the GLI motion relative to the micropipette. To measure it, the tracking of the micropipette and GLI need to be conducted first. Although the tilted tip of the micropipette is a region that can be detected to track the movement of the micropipette, it was covered by cytoplasm after ZP penetration which usually has poor optical transparency, making the localization of the micropipette a challenging task after ZP penetration. Except for the tilted tip, there are no significant feature points on the micropipette facilitating the track of

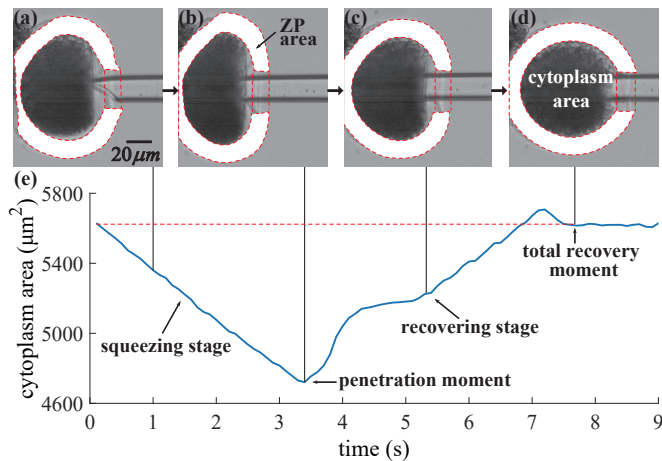


Fig. 4. Cell deformation detection results during the intracellular measurement process. The obtained ZP area in the (a) squeezing stage, (b) penetration moment, (c) recovering, and (d) total recovery. (e) The variation trend of cytoplasm area during cell penetration.

the micropipette. Addressing this, a marker, chosen from appropriately sized granulosa cells in the culture medium, is attached to the measurement micropipette. The detailed description of attaching the marker can be found in the "Supplementary file.doc" under the section "Marker Formation on Micropipette". The marker is utilized to localize the micropipette indirectly as it usually has no relative movement to the micropipette tip. Then the template of the micropipette marker and GLI were selected through mouse dragging and utilized to localize the micropipette and GLI as shown in Fig. 5(a).

Considering the size of the porcine oocytes (usually with a diameter of 130-160 μm), the 10x objective lens was chosen to image the oocyte and the GLI in the same field of view. For the captured images with a resolution of 720 × 480 in this field of view, the relative movement of the GLI and the micropipette was only a few pixels to tens of pixels (0.625 μm/pixel). To improve tracking precision, bilinear interpolation was used for image preprocessing to achieve sub-pixel GLI movement precision. Then template matching algorithm was used to track the absolute positions of the GLI and the micropipette, from which the relative movement of the GLI to the micropipette was obtained as the moving distance of the GLI in the micropipette during penetration (see Fig. 5(b)). It can be found that the moving distance of the GLI in the micropipette starts to increase after the ZP penetration moment, arrives at its peak after penetration, decreases in the recovering stage of the cell deformation, and finally stops at a constant value after the cell deformation fully recovers. Then the constant value is obtained to be ΔL in (11).

D. Robotic Measurement Process of Intracellular Pressure for Batch Oocytes Based on Improved Balance Model

After the target oocyte, measurement micropipette, and holding micropipette are positioned in the field of view, the system automatically autofocuses and then 3-D localizes them according to the imaging processing method reported previ-

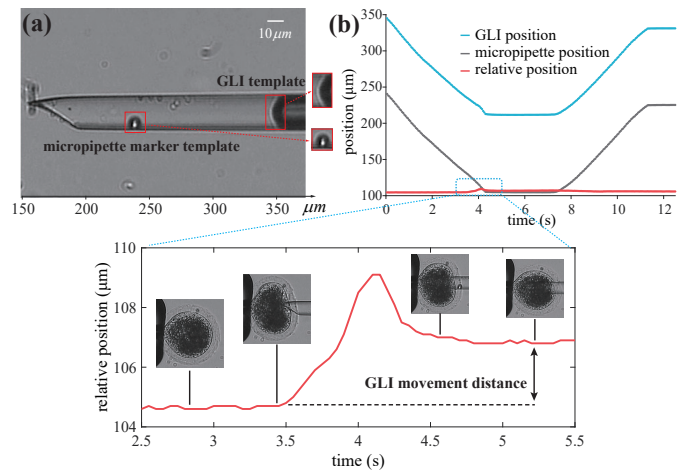


Fig. 5. Calculation results of the GLI moving distance during the intracellular measurement process. (a) The obtained micropipette marker template and GLI template. (b) The obtained relative position of GLI to micropipette equaling GLI moving distance inside micropipette during the intracellular pressure measurement.

ously [24], [30]. Then the system positions the measurement micropipette at the same height as the holding micropipette autofocuses it, and positions its central axes to coincide with that of the holding micropipette. After that, a positive pressure is increased to push the GLI into the field of view. Then, the operator selects the marker template and GLI template through mouse dragging. Then the robotic system automatically searches the whole area where target oocytes are stored and build a global map containing all oocytes through image stitching, and subsequently, localizes their positions and sorts them as introduced in our previously published paper [27].

After the above preparations work, the robotic system moves microstage to position one target oocyte into the field of view according to its located position on the global map. Then the system moves the holding micropipette to approach and aspirate it automatically according to their 3D positions. Further, the system moves the measurement micropipette to penetrate the ZP of the oocyte along the central axis of the micropipette and retreats it to let the cell deformation recover. During the above process, the cell deformation, measurement micropipette positions, GLI positions, and inner radius of the micropipette at GLI position were calculated in time using imaging processing methods. After the cell deformation fully recovers, the cell volume, the contact angle, and GLI moving distance inside the micropipette were calculated to obtain the intracellular pressure. After that, the system moves the microstage to the area for storing operated oocytes and releases the target cell with a positive pressure inside the holding micropipette. Then, if there is any oocyte left, the system moves microstage to position the next oocyte into the field of view, pick up it and repeat the above processes. The above robotic operation procedures were summarized in Fig. 6(a).

During the above robotic measurement process, the objective lens, pressure valve, microstage, holding micropipette, and measurement micropipette are moved coordinately through PID controllers to conduct the tasks including autofocusing of the oocyte and two micropipettes, picking up of the oocyte, ZP

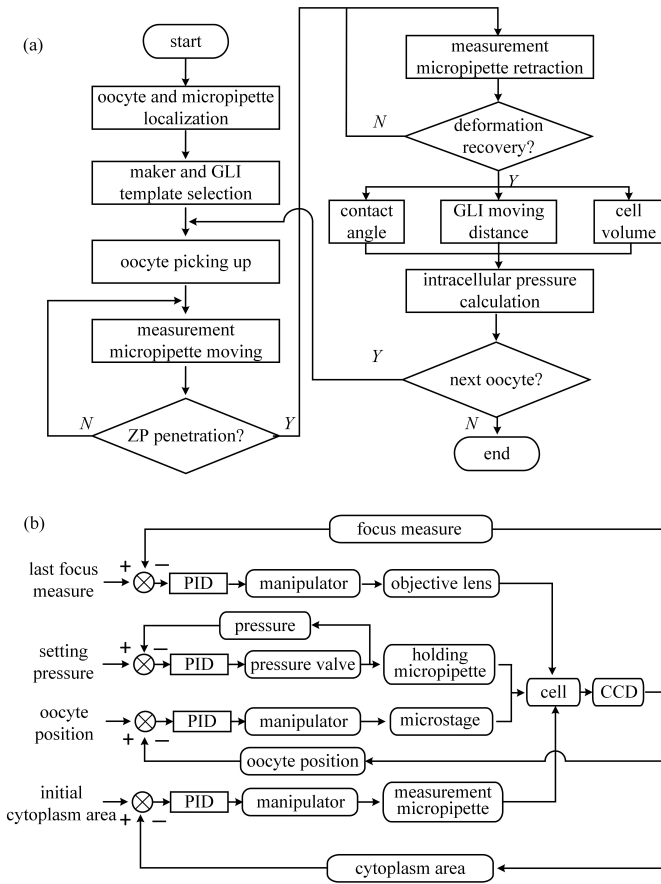


Fig. 6. Robotic measurement process of the intracellular pressure based on improved balance pressure model. (a) The operation flow of the robotic measurement of intracellular pressure. (b) The control diagram of the robotic intracellular pressure measurement system.

penetration, the retractions of the measurement micropipette and release of the oocyte. Imaging processing algorithms were utilized to calculate the key parameters of the improved balance pressure model required for intracellular pressure measurement. The control diagram of the robotic system is shown in Fig. 6(b). The mathematical derivations of the control loop related to the openness of the pressure valves (equation (A1) in reference [20]) and the motion of micromanipulators (equation (28) in reference [24]) have been included in our previous research.

IV. EXPERIMENTAL RESULTS

A total number of twenty MII-stage porcine oocytes were prepared to test the effectiveness of the work introduced in Section III. First, ten of twenty oocytes were measured by the robotic procedure shown in Fig. 6(a) to validate the feasibility of the proposed intracellular pressure measurement method. Pressure-leaking tests were then performed on the other ten oocytes to evaluate the measurement accuracy of the proposed method. Finally, the operated oocytes were observed after two hours of culture to evaluate their viability after the operation.

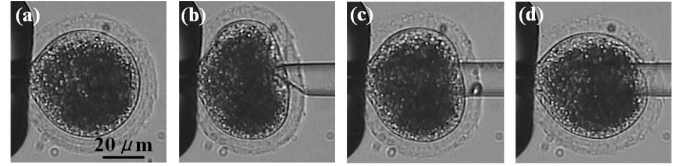


Fig. 7. Cell images during robotic measurement process of the intracellular pressure based on improved balance pressure model. (a) Before contact. (b) ZP penetration. (c) Recovering process. (d) Full recovery.

A. Intracellular Pressure Measurement Results

A number of ten porcine oocytes were measured using the proposed intracellular pressure measurement method. After the target oocyte was immobilized by the holding micropipette, the measurement micropipette was controlled to contact the oocyte, penetrate ZP, and retreat until the cell deformation recovered totally. Fig. 7 shows the cell images of one oocyte during the measurement process.

During the measurement process, the cytoplasm area, and motion of GLI and micropipette were measured in time using image processing methods introduced in Section III. The reader may find more details about the measured results in time in the supplementary video "In-time calculation results of key parameters.mp4". After the cell deformation fully recovered, the contact angle between the micropipette wall and the GLI, β , was calculated. Together with the radius of the micropipette R , the moving distance of GLI inside micropipette ΔL , the size of the tilted micropipette tip L_{in} , the cell volume obtained by cell radius R_{cell} , and the injection pressure P_{inj} , the cell inner pressure P_{in} was calculated. The obtained results of the above parameters are summarized in Table II.

In a series of experiments, some important parameters were statistically analyzed to guide the experiments. These parameters, including penetration speed, penetration depth, deformation recovery rate, micropipette retract distance, GLI moving distance and contact angle, are listed in Table SI in the "Supplementary file.doc." These data served as references for the cellular state and measurement effectiveness. The measured results are considered valid when most of the experimental parameters closely align with those in Table SI. When significant deviations from the reference parameters occur, such as the absence of cell deformation, penetration failure, or incomplete deformation recovery, the system will give a hint to the operator to interrupt the current measurement process to identify and address potential issues. The troubleshooting methods related to each parameter are also listed in Table SI.

It can be found that the obtained intracellular pressure of the fourth and seventh oocytes are negative values, which are apparently false results. According to the observation results from an embryo technician with more than 20 years of experience, the fourth oocyte is recognized to be a dead one with an extremely abnormal soft body, making ZP not penetrable even the tip of the measurement micropipette had almost touched the holding micropipette opening. In this matter, a negative calculation value of L_{in} is obtained, finally resulting in the negative intracellular pressure of the fourth oocyte. For the seventh oocyte, we found that one stain on

TABLE II
INTRACELLULAR PRESSURE MEASUREMENT RESULTS

	P_{inj} (hPa)	β ($^\circ$)	ΔL (μm)	L_{in} (μm)	R_{cell} (μm)	R (μm)	P_{in} (hPa)
1	91.81	51.10	1.13	7.50	56.56	10.63	5.75
2	93.22	50.81	0.44	18.75	51.88	10.63	6.63
3	93.42	51.53	1.88	25.63	55.10	10.63	8.17
4	93.46	30.90	0.06	-8.13	52.19	10.63	-24.13
5	101.26	44.56	0.63	30.00	56.88	10.63	3.62
6	106.23	43.62	2.06	23.13	56.56	10.63	7.03
7	107.11	30.41	1.31	32.50	52.81	10.63	-11.07
8	95.27	49.36	0.75	32.56	53.75	10.63	6.02
9	94.32	50.55	0.81	18.75	55.31	10.63	7.25
10	92.65	51.29	2.31	28.13	55.31	10.63	6.95

the micropipette surface occlude part of the GLI contour after cell deformation recovery was detected, which leads to a large fitting error of the contact angle β and subsequently, causing a false calculation result of the negative pressure. Apparently, abnormal situations similar to those of the above two oocytes can be prevented in the future after the target oocyte selection and clearance of the measurement micropipette before experiments. Except for the above two oocytes, the measured results of the rest 8 oocytes were all in accordance with the intracellular pressure ranges reported in related references [12], [14], [15], [19] with an average value of 6.43 ± 2.81 hPa ($n=8$), proving the feasibility of the proposed measurement method. The measurement success rate of the proposed method is up to 80%.

The average operation time for each cell from cell picking up to intracellular pressure calculation is only 12.0 ± 3.1 ($n=10$) seconds/cell. Although the 3D localization time of the two micropipettes and oocytes before oocyte picking up usually costs about 1 minute, it is only conducted once for the same batch of oocytes. Thus, it has limited influence on the average measurement speed of oocytes, especially when the number of measured oocytes is large. The measurement efficiency of our method is significantly higher than those methods relying on micropipette electrode resistance which is expected to measure only dozens of cells at most per day [21].

B. Intracellular Pressure Leaking Testing Results during the Measurement Process

During the cell penetration process, the ZP and outside wall of the micropipette need to be well sealed to avoid leakage of intracellular pressure. Otherwise, the leakage of intracellular pressure leads to a falsely smaller value of measured intracellular pressure than its original one. Appropriate penetration speeds of the measurement micropipette also need to be determined to reduce the probability of leakage. In this part, the fluorescent dye solution back-filling into the micropipette was injected into cells after ZP penetration to detect possible leakage of intracellular pressure (see Fig. 8(a)) during measurement.

First, a fluorescent dye (HTPS, 1mM) solution was back-filled into the micropipette. After the ZP penetration, the culture medium around the cell was replaced by a clean one to exclude the potential dye leakage before ZP penetration. Then, a positive pressure pulse was exerted inside the micropipette

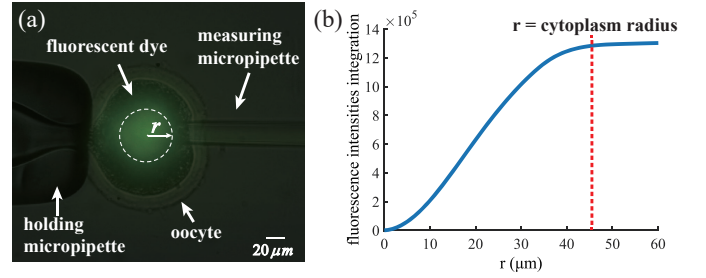


Fig. 8. Intracellular pressure leaking testing. (a) The combined cell image in the bright and fluorescent field of view. (b) The integration of fluorescence intensity at different radii.

to deposit a 2 pL volume of solution, only about 0.25% of the total volume of the oocyte calibrated by the method mentioned in previous research [31]. Then the field of view switches between the fluorescent field and bright field to check the scope of the fluorescent dye during the whole measurement process.

According to Lambert-Beer's law [32], the brightness of the fluorescence in the image is directly proportional to the concentration of the fluorescent dye. In the circular regions centered around the cell's centroid with varying radii, the fluorescence intensity was calculated through integration (see Fig. 8(b)). This integration enabled the quantification of the total amount of fluorescent dye within the regions of different radii. The experimental results on 10 oocytes indicated that the majority of the fluorescent dye is confined within the cell, with minimal to no increase in fluorescent dye beyond the cell's radius, which means no leakage of intracellular pressure during the measurement process (see Fig. 8(b)), guaranteeing the measurement accuracy of the intracellular pressure using our method. The above results also prove the feasibility of the diameter and penetration speed selection of the measurement micropipette (20 μm and 50 μm per second respectively) for intracellular pressure measurement.

C. Cell Viability Testing Results after Intracellular Measurement

The survival rate of the operated oocyte was tested after intracellular pressure measurement to evaluate the harm caused by the proposed method to the oocyte viability. The operated oocyte is considered to survive if the cytoplasm edge is observed to recover to an integrated and clear state (see Fig. 9(a)-(c)) during 2 hours of culture. If the edge of the cytoplasm dose not recover, the viability of the oocyte is considered to be damaged and the oocyte may be dead. According to the observation results, only one oocyte out of the eight successfully measured was found to have an unsmooth cytoplasmic edge near the wound. The above results demonstrate that the survival rate of the oocyte measured by the proposed method is up to 87.5% (7/8), proving limited harm to cell viability.

V. DISCUSSIONS

In comparison to most intracellular pressure measurement methods relying on specific and expensive devices, the pro-

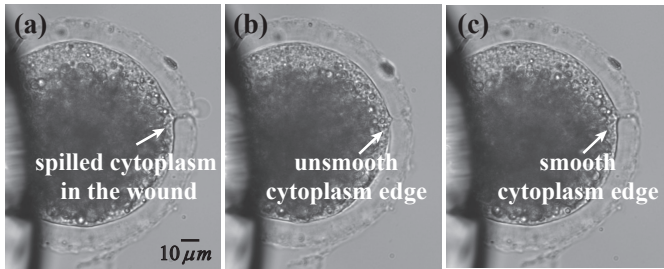


Fig. 9. The oocyte image during 2 hours of culturing after the measurement. (a) The oocyte image right after the measurement, with visible spilled cytoplasm in the wound on the zona pellucida. (b) The oocyte image after 1 hour of culturing following the measurement, with no visible cytoplasm in the wound on the zona pellucida, but the cytoplasmic edge near the wound remains unsmooth. (c) The oocyte image after 2 hours of culturing following the measurement, with no visible cytoplasm in the wound on the zona pellucida, and the cytoplasmic edge near the wound has smoothed out.

posed robotic intracellular pressure measurement method can be achieved based on the traditional cell injection system setup. In this method, the measurement micropipette penetrates the ZP of the oocyte to sense the intracellular pressure. As the ZP penetration operation is the first required step for many manipulation tasks of oocytes/embryos such as cell microinjection, the proposed method is able to achieve in-situ measurement of intracellular pressure before cell manipulation. This advantage of our method is vital for reducing the disturbances of intracellular pressure to manipulation results such as the injection volume. Besides, in comparison to our previous intracellular pressure method based on the volume of oil injected into cells, the proposed method does not deposit any harmful materials into the intracellular space during the measurement process. This advantage is vital for keeping the viability of the operated cell.

As our method is an invasive measurement, the intracellular pressure will be released from the cut generated in ZP penetration after the measurement micropipette retreats out of the cell. Thus, after being measured by our method, the intracellular pressure does not exist again, making it impossible to be measured again by the other methods. To benchmark our method and evaluate its measurement error, our method will be applied to cells without ZP in the future. For these cells, their intracellular pressure will be first noninvasively measured by the cortical tension of the cell [13], [14]. Then these cells will be measured by our method. In this way, the measurement accuracy of our method can be evaluated through the comparison between the obtained results using two methods for the same cell.

Theoretically, through the back-and-forth motion of the measurement micropipette inside the cell, the intracellular pressure measurement can be repeated if an effective seal between the ZP and the outside surface of the micropipette maintains. Unfortunately, we found that the seal between the ZP and the outside wall of the micropipette easily breaks under multiple back-and-forth motions of the measurement micropipette inside the oocyte. Thus, the repeatability test of our measurement method is still a challenging task before an effective method to maintain the intracellular pressure is

developed in the future.

The main measurement error of the proposed method results from the calculation error of P_{inj} , β , R , V_{tip} , and V_{cell} . Among them, P_{inj} has been calculated indirectly by the openness degree of the valve according to the calibrated relationship between them [20]. Through this method, the resolution of P_{inj} can be improved to 0.1 Pa level. Thus, the influence of P_{inj} on the measurement error of the intracellular pressure is rather limited. In comparison to P_{inj} , the other four parameters are calculated through image processing methods. The imaging resolution has a significant influence on the measurement errors of them. Equipping microscopes and cameras with higher imaging resolution may improve the measurement accuracy of these parameters in the future.

Besides, only twenty oocytes were tested due to the influence of the Covid-19 epidemic during our research period. More cells will be measured in the future to further validate the effectiveness of the proposed method in this paper.

VI. CONCLUSIONS

This paper presented a robotic intracellular pressure measurement method based on an improved balance pressure model. With the traditional cell manipulation tools and devices, this method is demonstrated to measure porcine oocytes with an 80% success rate at an average speed of 12s /cell. With improvement in the selection of oocyte and measurement micropipette, the success rate can be further improved in the future. Besides, no observable intracellular pressure leakage was found through fluorescent dye injection after ZP penetration. Moreover, the operated cells have a high survival rate of 87.5% after measurement. The independence from specific and expensive devices and low harm to cell viability enable our method high applicability in biological applications requiring in situ measurement of intracellular pressure.

REFERENCES

- [1] J. D. Szafranski, A. J. Grodzinsky, E. Burger, V. Gaschen, H.-H. Hung, and E. B. Hunziker, "Chondrocyte mechanotransduction: effects of compression on deformation of intracellular organelles and relevance to cellular biosynthesis," *Osteoarthritis and cartilage*, vol. 12, no. 12, pp. 937-946, 2004.
- [2] S. A. Gudipaty et al., "Mechanical stretch triggers rapid epithelial cell division through Piezo1," *Nature*, vol. 543, no. 7643, pp. 118-121, 2017.
- [3] Z. Tang et al., "Mechanical forces program the orientation of cell division during airway tube morphogenesis," *Developmental cell*, vol. 44, no. 3, pp. 313-325. e5, 2018.
- [4] G. H. Altman et al., "Cell differentiation by mechanical stress," *The FASEB Journal*, vol. 16, no. 2, pp. 1-13, 2002.
- [5] D. Dado, M. Sagi, S. Levenberg, and A. Zemel, "Mechanical control of stem cell differentiation," *Regenerative medicine*, vol. 7, no. 1, pp. 101-116, 2012.
- [6] W. Strychalski and R. D. Guy, "Intracellular pressure dynamics in blebbing cells," *Biophysical journal*, vol. 110, no. 5, pp. 1168-1179, 2016.
- [7] R. J. Mogil et al., "Effect of low-magnitude, high-frequency mechanical stimulation on BMD among young childhood cancer survivors: a randomized clinical trial," *JAMA oncology*, vol. 2, no. 7, pp. 908-914, 2016.
- [8] F. Wo et al., "A multimodal system with synergistic effects of magneto-mechanical, photothermal, photodynamic and chemo therapies of cancer in graphene-quantum dot-coated hollow magnetic nanospheres," *Theranostics*, vol. 6, no. 4, p. 485, 2016.
- [9] K. H. Vining and D. J. Mooney, "Mechanical forces direct stem cell behaviour in development and regeneration," *Nature reviews Molecular cell biology*, vol. 18, no. 12, pp. 728-742, 2017.

- [10] M.-D. Nguyen et al., "Effects of physiologic mechanical stimulation on embryonic chick cardiomyocytes using a microfluidic cardiac cell culture model," *Analytical chemistry*, vol. 87, no. 4, pp. 2107-2113, 2015.
- [11] M. Knoblauch, J. M. Hibberd, J. C. Gray, and A. J. van Bel, "A galinstan expansion femtosyringe for microinjection of eukaryotic organelles and prokaryotes," *Nature biotechnology*, vol. 17, no. 9, pp. 906-909, 1999.
- [12] X. Wang et al., "Effect of cell inner pressure on deposition volume in microinjection," *Langmuir*, vol. 34, no. 35, pp. 10287-10292, 2018.
- [13] R. P. Rand and A. Burton, "Mechanical properties of the red cell membrane: I. Membrane stiffness and intracellular pressure," *Biophysical journal*, vol. 4, no. 2, pp. 115-135, 1964.
- [14] C. J. Chan et al., "Hydraulic control of mammalian embryo size and cell fate," *Nature*, vol. 571, no. 7763, pp. 112-116, 2019. DOI: 10.1038/s41586-019-1309-x.
- [15] X. Wang, Z. Zhang, H. Tao, J. Liu, S. Hopyan, and Y. Sun, "Characterizing inner pressure and stiffness of trophoblast and inner cell mass of blastocysts," *Biophysical journal*, vol. 115, no. 12, pp. 2443-2450, 2018.
- [16] R. J. Petrie, H. Koo, and K. M. Yamada, "Generation of compartmentalized pressure by a nuclear piston governs cell motility in a 3D matrix," *Science*, vol. 345, no. 6200, pp. 1062-1065, 2014.
- [17] Y. Lu et al., "Macula densa nitric oxide synthase 1 β protects against salt-sensitive hypertension," *Journal of the American Society of Nephrology*, vol. 27, no. 8, pp. 2346-2356, 2016.
- [18] R. J. Petrie, H. M. Harlin, L. I. T. Korsak, and K. M. Yamada, "Activating the nuclear piston mechanism of 3D migration in tumor cells," *Journal of Cell Biology*, vol. 216, no. 1, pp. 93-100, 2017.
- [19] M. Li et al., "Robotic Intracellular Pressure Measurement Using Micropipette Electrode," *Sensors*, vol. 23, no. 10, p. 4973, 2023.
- [20] Q. Zhao et al., "A novel pneumatic micropipette aspiration method using a balance pressure model," *Review of Scientific Instruments*, vol. 84, no. 12, p. 123703, 2013.
- [21] R. J. Petrie and H. Koo, "Direct measurement of intracellular pressure," *Current protocols in cell biology*, vol. 63, no. 1, pp. 12.9. 1-12.9. 9, 2014.
- [22] Y. Sun, Y. Liu, Q. Zhao, M. Sun, and X. Zhao, "Modeling and measuring intracellular displacement during cell penetration," *Journal of Applied Physics*, vol. 127, no. 4, p. 044701, 2020.
- [23] Q. Zhao et al., "Robotic label-free precise oocyte enucleation for improving developmental competence of cloned embryos," *IEEE Transactions on Biomedical Engineering*, vol. 68, no. 8, pp. 2348-2359, 2020.
- [24] Q. Zhao, M. Sun, M. Cui, J. Yu, Y. Qin, and X. Zhao, "Robotic cell rotation based on the minimum rotation force," *IEEE Transactions on Automation Science and Engineering*, vol. 12, no. 4, pp. 1504-1515, 2014.
- [25] A. Zhang, X. Zhao, M. Wu, and X. Feng, "Coating method of micro pattern based on microscopic injection system," in *2013 International Conference on Manipulation, Manufacturing and Measurement on the Nanoscale*, 2013: IEEE, pp. 309-313, 2013.
- [26] Y. Zhang et al., "Mechanical Force Estimation Based on Visual Cell Deformation and Improved Point-Load Model," *IEEE Transactions on Instrumentation and Measurement*, vol. 72, pp. 1-9, 2023.
- [27] Q. Zhao, M. Cui, C. Zhang, J. Yu, M. Sun, and X. Zhao, "Robotic enucleation for oocytes," in *The 9th IEEE International Conference on Nano/Micro Engineered and Molecular Systems (NEMS)*, 2014: IEEE, pp. 23-27.
- [28] Q. Zhao et al., "Robotic Patch Clamp Based on Noninvasive 3-D Cell Morphology Measurement for Higher Success Rate," *IEEE Transactions on Instrumentation and Measurement*, vol. 71, pp. 1-12, 2022.
- [29] Y. Liu et al., "Oocyte orientation selection method based on the minimum strain position in the penetration process," *Journal of Applied Physics*, vol. 125, no. 15, 2019.
- [30] Z. Wang, C. Feng, W. T. Ang, S. Y. M. Tan, and W. T. Latt, "Autofocusing and polar body detection in automated cell manipulation," *IEEE Transactions on Biomedical Engineering*, vol. 64, no. 5, pp. 1099-1105, 2016.
- [31] J. Liu, V. Siragam, J. Chen, M. D. Fridman, R. M. Hamilton, and Y. Sun, "High-throughput measurement of gap junctional intercellular communication," *American Journal of Physiology-Heart and Circulatory Physiology*, vol. 306, no. 12, pp. H1708-H1713, 2014.
- [32] J. Li, Y. Tong, L. Guan, S. Wu, and D. Li, "A turbidity compensation method for COD measurements by UV-vis spectroscopy," *Optik*, vol. 186, pp. 129-136, 2019.



Jinyu Qiu received the B.Eng. degree in automation from Taiyuan University of Technology, Taiyuan, China, in 2019. He is currently pursuing his Ph.D. degree with the College of Artificial Intelligence, Nankai University. He was also a visiting student at Imperial College London from 2022 to 2023. His research interests include robotic patch clamp system, micromanipulators and microsystems.



Minghui Li received a bachelor's degree in mechanical engineering from Beijing Jiaotong University in 2021. She is currently studying for a master's degree in control science and engineering at Nankai University. Her research interests include micromanipulators and microsystems.



Ruimin Li received the B.Eng. degree in Intelligence Science and Technology, Hebei University of Technology, Tianjin, China, in 2022. She is currently pursuing her Ph.D. degree in control science and engineering with Nankai University, Tianjin, China. Her research interests include robotic patch clamp system, micromanipulators and microsystems.



Yue Du is a lecturer at the Artificial Intelligence College of Nankai University. After receiving a Ph.D. from the National University of Singapore in 2015, she pursued a postdoctoral study at the University of Oklahoma. She has carried out in-depth research in the intersection of engineering, biology and medicine, such as micro-manipulation robot systems, smart medicine and biophysical analysis.



Yaowei Liu (Member, IEEE) received the B.Eng. degree in automation and the Ph.D. degree in control theory and control engineering from Nankai University, Tianjin, China, in 2013 and 2019, respectively. He is currently a Post-Doctoral Fellow with the College of Artificial Intelligence, Nankai University. He is also with the Institute of Intelligence Technology and Robotic Systems, Shenzhen Research Institute of Nankai University, Shenzhen, China. His research interests include micromanipulators and microsystems.



Mingzhu Sun (Member, IEEE) received the B.S., M.S., and Ph.D. degrees in computer science and technology, computer application, control theory, and control engineering from Nankai University, Tianjin, China, in 2003, 2006, and 2009, respectively.

Since 2009, she has been with the Institute of Robotics and Automatic Information System and the Department of Automation and Intelligence Science, Nankai University, Tianjin, China. She is currently an Associate Professor in micro-manipulation. Her

research interests are in micromanipulator for life science, image processing, and computer vision.



Xin Zhao (Member, IEEE) received the B.S. degree from Nankai University, Tianjin, China, in 1991, the M.S. degree from the Shenyang Institute of Automation, CAS, Shenyang, China, in 1994, and the Ph.D. degree from Nankai University in 1997, all in control theory and control engineering. He joined the faculty at Nankai University in 1997, where he is currently a Professor and the Dean of the College of Artificial Intelligence. His research interests are in micromanipulator, microsystems, and mathematical biology.



Qili Zhao (Member, IEEE) received the Ph.D. degree in control theory and control engineering from Nankai University, Tianjin, China, in 2014. He finished his first post-doctoral research with the Robotics and Mechatronics Research Laboratory, Department of Mechanical and Aerospace Engineering, Monash University, Melbourne, VIC, Australia, from 2014 to 2015 and was a Post-Doctoral Fellow with the Advanced Micro and Nanosystems Laboratory, Department of Mechanical and Industrial Engineering, Toronto University, Toronto, ON, Canada,

from 2015 to 2018. He is currently an Associate Professor with the College of Artificial Intelligence, Nankai University. His research interests include robotic patch clamp, robotic cell manipulation, and robotic cell measurement.